Energy & Environmental Science

ROYAL SOCIETY OF CHEMISTRY

PAPER

View Article Online
View Journal | View Issue

Cite this: *Energy Environ. Sci.*, 2025, **18**, 884

Arbitrary and active colouring of solar cells with negligible loss of efficiency†

Yan-Song Zhang, ‡ Hasan Arif Yetkin, ‡ Hakam Agha, Sevan Gharabeiki, Rijeesh Kizhakidathazhath, Lena Merges, Ricardo G. Poeira, Jan P. F. Lagerwall * and Phillip J. Dale *

While the current surging global energy crisis highlights the urgent need for a transition to renewable energy sources, the large physical footprint—as experienced by humans—of the required installations reduces public acceptance and therefore strongly hampers its development. Solar modules, for electricity and/or for heating, do not have the audible impact of wind turbines but their visible impact is currently prohibitive for many installation options, such as on the façades of buildings. Here we show that coatings of cholesteric liquid crystals (CLCs) can turn any black solar modules into passive surfaces with arbitrary colour or active surfaces with temperature sensitive colouration, yet with minimum loss of power conversion efficiency (PCE), thanks to their self-organized helical modulation generating structural colour. Most conspicuously, we combine red, green, and blue pixels to generate a non-spectral colour that blends into wooden or metallic backgrounds with a 50% relatively higher PCE than a ceramic ink equivalent since CLCs neither absorb nor scatter light. Further, we show thermochromic solar cells with colour tunable across the full visible spectrum, maintaining 88% of their original PCE. We argue these coatings can be developed to cover solar modules with either arbitrary full-colour images, allowing them to be aesthetically integrated into building façades and roofs in a way that is fully acceptable by the public, or with active colour changing to add functional value, while always keeping high PCE.

Received 9th July 2024,
Accepted 25th November 2024

DOI: 10.1039/d4ee03010a

rsc.li/ees

Broader context

Currently, the world's energy infrastructure is almost invisible to the human eye because of the high energy density of fossil fuels. Switching from centralized thermal power stations to decentralized wind and solar photovoltaic modules to generate our electricity, the infrastructure will become visibly inescapable in its current form. In areas with high population and energy demand, calculations show that a land coverage of ~6% of photovoltaic modules will be required. Protests against large-scale photovoltaic installations are manifesting. Camouflaging the modules into the urban environment on roofs, façades, and vertical surfaces is a solution to this problem. Camouflaged ceramic ink covered modules are possible, but the energy yield is significantly reduced. Structurally coloured modules are only available in monotone colours, making them difficult to integrate. Using cholesteric liquid crystals as a colouring layer, we show solar cells with a high retained power conversion efficiency with the ability to be patterned so that they disappear from sight when placed against building materials. We even show solar cells with active temperature responsive colouring across the visible spectrum. Using these liquid crystal coatings with integrated photovoltaics, we can convert our urban cityscapes into energy generating surfaces, which seamlessly fit into their environment.

Introduction

Climate change requires that we transition from a world powered by carbon emitting fossil fuel to one where we harvest energy from renewable sources without emission of greenhouse gases. The sixth assessment report of the Intergovernmental Panel on Climate Change makes clear that wind and solar energy technologies offer the biggest potential to reduce carbon emissions by far and, encouragingly, they are also the cheapest.[1] Two groundbreaking studies of how our planet could run on 100% renewable energy found for Belgium, Luxembourg, and the Netherlands (exemplary countries with high population density and high energy demand), that between 2 and 6% of their respective land surface would need to be covered with photovoltaic (PV) modules in addition to wind turbines.[2,3] To put this in perspective, the average

University of Luxembourg, Department of Physics & Materials Science, 1511 Luxembourg, Luxembourg. E-mail: phillip.dale@uni.lu, jan.lagerwall@lcsoftmatter.com

† Electronic supplementary information (ESI) available. See DOI: https://doi.org/10.1039/d4ee03010a

‡ These authors contributed equally to this work.

percentage of man-made surface of these countries is 11%, which is nearly the highest in Europe.[4] This additional large area of modules would lead to cityscapes and some part of the landscapes appearing monotonously black in colour, if conventional PV technology were used. Furthermore, although solar energy is generally perceived positively, large PV module installations have received negative feedback from the public.[5] One way to overcome these potential drawbacks and improve public acceptance is to colour the PV modules or even camouflage them into their surroundings.

Colour plays a profound and multifaceted role in shaping our perception of the world around us. Its effects are not only visual but also extend into our psychological and physiological experiences. To date, coloured PV modules have been developed mainly within the scope of building integrated photovoltaic (BIPV) applications. These are PV modules that have a dual use as energy generator and building element. Since buildings account for 40% of final energy use it makes great sense not only to use roofs but also the façades for generating energy.[6–8] If BIPV can be realized such that it gives a significant contribution to the energy supply and decentralisation of energy systems, it would reduce the amount of utility-scale PV that will have to be placed in non-urbanized spaces. Colouring BIPV improves the possibility of fitting modules into their local environment in a visually pleasing way, see concept in Fig. 1, thereby enabling more of the building's visible surface to be used to generate energy.[9] To allow any façade section exposed to sunlight to be used, it is not enough to make monocoloured modules with a limited palette, because in many cases truly aesthetic integration requires arbitrary colours as well as patterning. Of course the additional colouring of the module should not inhibit an effective generation of electrical power. In fact, there is a trade-off between colouring a PV module and its ability to generate power efficiently, and this greatly depends on *how* the colour is generated; any effect other than reflection of the desired colour, such as absorption or indiscriminate scattering, must be avoided to minimise the negative impact on PV performance.

The two most popular ways to colour PV modules are either to apply multi-layer thin film stacks giving rise to structural colour by interference or to use standard pigments dispersed in an ink, generating colour as a result of absorption and scattering. The multi-layer structures are designed to have regular changes in refractive index on the scale of light wavelengths, causing a Bragg like reflection of light within a specific colour band. This allows the rest of the solar radiation to transmit through to the underlying solar cells, hence minimising impact on solar to electrical power conversion efficiency (PCE). These multi-layers are grown by vacuum deposition systems over large areas, the size of the module, to create constant colour whilst keeping a power output of over 90% of the original uncoloured module.[10,11] The disadvantages are that

1. it is challenging to pattern the solar cell in order to go beyond the mono-colour PV category.

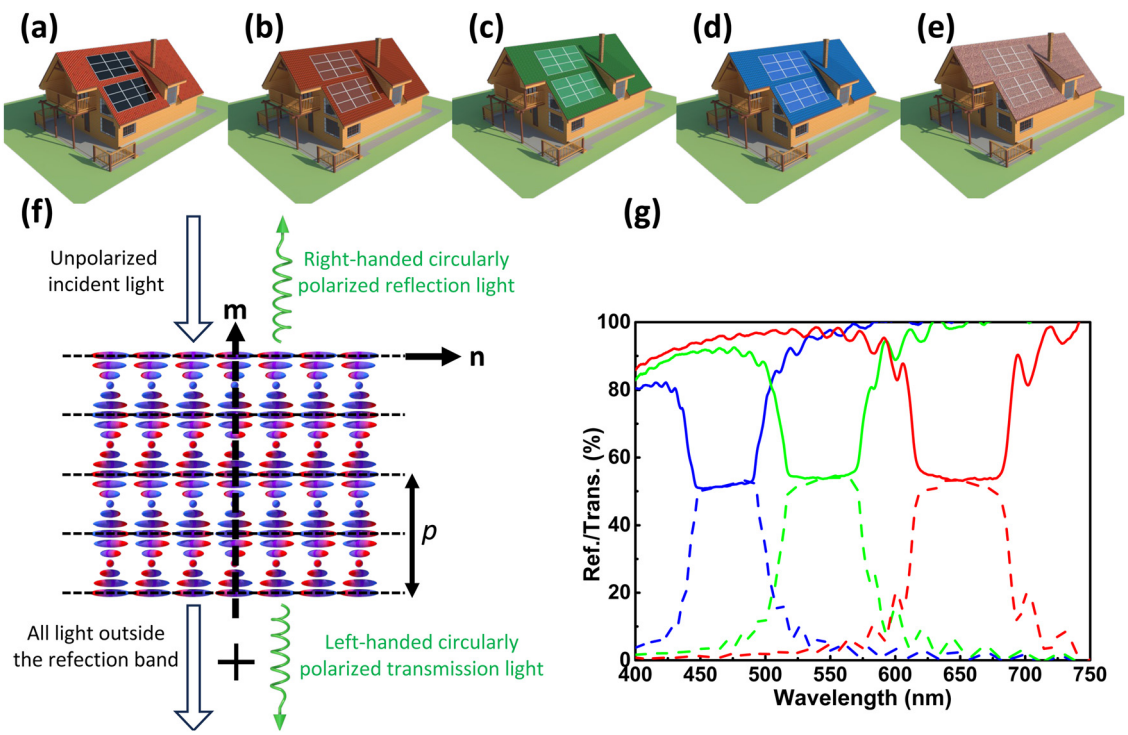

Fig. 1 (a) Roof PV installations of today. (b)–(d) Monocolour BIPV modules with near matching roof colour. (e) With full-colour patterning, BIPV can be seamlessly integrated with arbitrary roofs. (f) Schematic illustration of the local helicoidal order modulation in cholesteric liquid crystals, defining the director **n**, the helix axis **m** and the helix pitch *p*. The selective reflection and complete transmission outside the reflection band are illustrated for the case of green right-handed retroreflection. (g) Measured transmission (continuous lines) and reflection (dashed lines) spectra of CLC mixtures tuned for red (R), green (G), and blue (B) retroreflection (see Table S1, ESI† for compositions) filled into standard LC cells with parallel flat glass plates 15 μm apart.

2. the obtainable colour palette does not include all colours that our eyes can perceive.

3. the colour is viewing and illumination angle-dependent, such that the actual colour of the module appears different if mounted on a vertical wall or inclined roof, and for either case the colour will also change between a sunny day with directed illumination compared to a cloudy day with diffuse light.

Pigments in inks, on the other hand, can be deposited locally by liquid printing methods to create patterns or pictures with arbitrary colours, enabling them to truly camouflage PV modules into their environment.[12,13] But this enhanced colouring freedom comes at the cost of significantly reducing the PCE performance of PV modules by up to 68%, since the pigments absorb and scatter light that could have been used by the solar cells.[12,13] Combining the ability of inks to produce local colour variation with the optical efficiency of structural colour would enable a patterned picture or arbitrarily coloured BIPV modules with high PCE.

A more versatile approach to generate structural colour is to take advantage of the self-assembly provided by cholesteric liquid crystals (CLCs) to generate the periodic refractive index modulation required to generate visible Bragg diffraction. In CLCs, the molecules spontaneously align over large distances along a common orientation (indicated by the director, **n**) and this orientation continuously rotates in a helical fashion along a direction **m** $\perp$ **n**, see Fig. 1(f).[14,15] The long-range orientational order along **n** leads to optical anisotropy (birefringence) with a greater local refractive index $n_{\parallel}$ along **n** than $n_{\perp}$ perpendicular to it (or *vice versa*), such that the rotation along **m** results in the periodic modulation of the effective refractive index required for structural colour. As the name suggests, CLCs are liquid, enabling all types of liquid processing (including ink jet printing),[16–18] and by using reactive molecules the CLC mixture can be turned solid by polymerisation while retaining the self-assembled structure,[19] thus enabling the use of CLCs for templating solid and durable materials.[20] As with other types of structural colour, the selective reflection of CLCs is viewing angle-dependent, the centre wavelength of the reflection band being given by:

$$\lambda_r = \bar{n}p\cos\theta, \quad (1)$$

where $\bar{n} \approx 1.5$ is the average refractive index of the CLC, p is the pitch of the helical modulation, and θ is the viewing angle with respect to **m**. The longest reflected wavelength is thus seen at retroreflection ($\theta = 0$), the retroreflection wavelength being given by the simple relationship $\lambda_0 = \bar{n}p$. The width of the reflection band is given by:

$$p\Delta n \quad (2)$$

where $\Delta n \approx 0.1$ is the local birefringence of the CLC phase, as measured in the absence of helix.[15]

A key difference from other materials generating structural colour is that the chirality of a CLC helix selects only one handedness of circular polarisation for reflection: a right-handed CLC helix reflects all right-handed polarised light within the reflection band, but the left-handed light is passed through. This means that CLC-generated colour can have an exceptionally small impact on the performance of PV modules, since all light outside the reflection band and half the light within the reflection band is transmitted, since the incoming light is unpolarised, see Fig. 1(f). Bae *et al.* were the first to demonstrate the potential of CLCs for adding colour to solar cells, using prefabricated polymerised CLC films with constant red, green or blue colour that were glued on the outside of the front protective glass.[21] They chose to maximise colour intensity by sandwiching two identical left-handed CLC films around a thin film acting as a $\lambda/2$ plate, converting the right-handed polarised light transmitted by the first CLC film into left-handed, in order that all light within the reflection band was reflected. This of course came at the cost of reduced PCE of the solar cell.

Here, we take the first step in demonstrating the potential of CLCs to solve problems (1) and (2) mentioned above, by pixelating a reactive CLC film with temperature-tunable retroreflection colour, created by photocrosslinking different pixels at different temperatures using a photomask, thereby generating an array with red, green and blue retroreflection. We show that this allows us to generate non-spectral colours on solar cells to camouflage them with their surroundings, and we demonstrate that the impact on solar cell performances is minimal. We discuss problem 3, namely the angular instability of structural colour, and how this can be overcome. Finally, we also make uniformly coloured thermochromic CLC layers on solar cells that are not polymerised, and where the retroreflection colour can be tuned continuously from red to blue by changing the temperature. In all cases, we use a single layer of CLC and we coat this in the liquid state directly on the solar cell, below the protective top glass layer, and we demonstrate that this causes no damage. In fact, we argue that our approach of internal CLC colouring layer is ideal, as it protects the CLC film from weather impact and mechanical disturbance, it minimises losses due to scattering, and because the CLC film can be easily combined with the encapsulation elements against weather-related factors used in commercial silicon solar modules.

Results and discussion

Permanent CLC-generated single spectral colour solar cells

We first demonstrate the application of thermally stable permanently coloured CLCs directly on top of inorganic thin film $Cu(In,Ga)Se_2$ (CIGSe) based solar cells below the outer protective top glass. Fig. 2(a) displays the schematic of the device structure including CLC colouring layer. The full fabrication process is described in the Methods and Fig. S2 (ESI†). Briefly, we first attach the protective top glass plate to the solar cells, each plate nearly fully covering eight solar cells, using glue along two parallel sides of the glass. By including spacer balls in the glue, we fix the solar cell-to-protective glass spacing to 15 μm. We then place a drop of each reactive CLC mixture at an edge without glue, such that capillary forces suck the CLC into the interstitial space. After completing filling and annealing, the samples are exposed to ultraviolet (UV) light to photopolymerise the CLC into

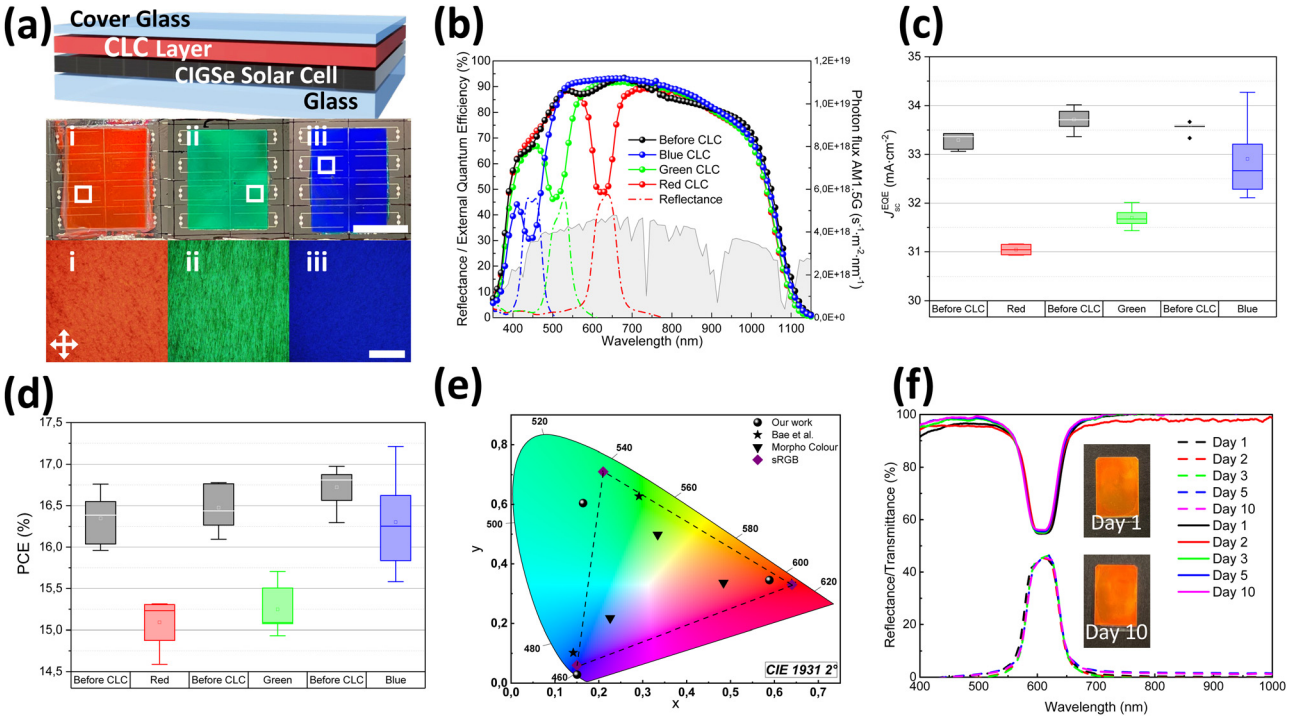

Fig. 2 (a) Top: Structural diagram of CIGSe solar cell with CLC colouring layer. Middle: Macroscopic photographic image of three samples with eight solar cells each, covered by polymerised CLC films generating red, green and blue retroreflection colour, respectively. Scale bar: 1 cm. Bottom: Close-up images obtained by reflection polarized optical microscopy (POM) of the sample areas marked by squares in middle. Scale bar: 200 μm. (b) Corresponding reflection spectra (dashed) and *EQE* spectra (continuous) of the most efficient type of each coloured solar cell (red, green, blue, as the respective retroreflection colour) along with the representation of the AM1.5G photon flux (grey shaded area) plotted against the right axis. A reference *EQE* spectrum of one of the cells without CLC in (a) is plotted in black. The box plot statistical properties of before and after CLC for red (4) green (8) and blue (5) solar cells (see Section SI 1.4 ESI†) with (c) displaying the J_{SC}^{EQE} and (d) showing the active area PCEs. (e) Colour coordinates comparison in the CIE 1931 2° chromaticity diagram between our three samples (black balls), Bae *et al.* (stars)[21] and Morpho colour (triangles),[11] as obtained from reflection spectra. The colour gamut of sRGB is shown with purple diamonds. (f) Ten days of monitoring results of transmission and reflection spectra of CLC films at 85 °C and 85% humidity. Photography images of the film before stability testing on the first day and on the tenth day of the stability test.

a solid film. In total, eight solar cells are assigned to each of the red, green and blue retroreflection colours, with the current density–voltage (*JV*) and external quantum efficiencies (*EQE*) of the solar cells being measured before the application of the CLC colouring layers to act as exact reference solar cells. All the reference solar cells before CLC coating have similar PV performances as shown in Fig. S4 (ESI†).

The bottom part of Fig. 2(a) shows reflection microscopy images (crossed linear polarisers) of the coloured solar cells. In each case they appear with one single bright colour, albeit with some very small regions that are dark which is likely where the CLC is locally misaligned and does not efficiently retroreflect the light. The reflectance spectra of the coloured solar cells show each of them having a single peak with a maximum reflectance of ∼48% (see Fig. 2(b)), which is almost the maximum possible for a single layer of CLC, slightly higher than the single-layer reflectance of Bae *et al.*[21]

Wavelength dependent *EQE* measurements assess the effect of the colouring layers on the current collecting ability of the solar cells and are shown in Fig. 2(b). The reference measurement shown here was obtained from one of the reference solar cells before the CLC coating devoid of any cover glass, exhibiting a typical *EQE* spectrum for CIGSe solar cells with an *EQE* of greater than 80% above the band gap, observed here around 1100 nm. At wavelengths shorter than 530 nm the *EQE* decreases down to 10% due to the parasitic absorption of the buffer and window layers. Since our CLC colouring layer allows all photons to pass through to the solar cells to generate charge carriers except those that are reflected by the CLC, *i.e.*, those with wavelength within the local reflection band and the same circular polarisation handedness as the CLC helix, we expect to observe similar *EQE* spectra for the coloured solar cells as the reference except for a dip in the respective reflection band. This is indeed what is observed, with the red, green, and blue solar cells all showing narrow dips in the *EQE* of around 40%. The lack of any other dips confirms the absence of parasitic absorption or scattering in other wavelength regions, in stark contrast to non-structural colouring methods. Remarkably, outside of the CLC selective reflection dip in the *EQE* spectrum, each coloured solar cell shows a slightly higher response than the non-coloured one, most likely due to better refractive index matching between the different layers on top of the solar cells (see Section SI 1.5, ESI† for the effect of the cover glass on *EQE* spectra).

Multiplying the *EQE* spectrum by the sun's AM1.5G solar spectrum on earth and then integrating across the wavelength range enables us to calculate the short circuit current density (J_{SC}^{EQE}) of each solar cell, as if the entire surface is covered with the colouring layer (see Methods). Using this value of J_{SC}^{EQE} the light illuminated *JV* curves have been corrected for the coloured solar cells and also the uncoated reference solar cells (before CLC) and all other PV parameters were recalculated. Therefore, it is important to note that the (power conversion efficiencies) PCEs shown in this study pertain to active area efficiency of solar cells. The coloured solar cells all show almost the same open circuit voltage (V_{OC}) and fill factor (*FF*) (see Fig. S3 and S4, ESI†) as compared to the reference measurements, demonstrating that the polymerised CLC layer has no detrimental electrical effect on the underlying solar cell. Only the J_{SC}^{EQE} values of the coloured cells are slightly reduced, as shown in Fig. 2(c), in order of blue, green, then red, which corresponds to the width of the reflection band (see eqn (2)) and the fact that the number of photons from the sun is the least in the blue part and the most in the red part of the solar spectrum (see Fig. 2(b)). Thus, the decrease in PCEs of the solar cells (see Fig. 2(d)) follow exactly the decrease in J_{SC}^{EQE}. Overall, the relative PCEs of the blue, green, and red best solar cells are 96.3, 93.6 and 92.6%, respectively, which is similar or slightly better than the best published inorganic Bragg filter[11] and the previously used free standing CLC film,[21] as shown in Table 1. When comparing power outputs, we should be mindful that the band gap of the absorbing layer of the solar cell plays a role. The same colouring layer on a high band gap solar cell will have a reduced power output compared to a low band gap solar cell, since the high band gap cell will absorb relatively fewer photons. Hence, for coloured solar cells low band gap photovoltaic absorber layers such as CIGSe and silicon (around 1.1 eV) have a competitive advantage over high band gap absorber layers such as hybrid-inorganic–organic–perovskites (1.5–1.65 eV). Table 1 displays also the relative PCEs of some of commercially available PV modules in red, green and blue colours. It is evident that our CLC colouring layers lead to considerably higher relative PCE than the ink based layers.

Besides the relative PCE, the other important property is the reflected light spectrum of the solar cell or the human perception of its colour, which is of great interest to architects. Several attempts have been made to correlate colour and PCE in a single figure of merit,[22–24] but as yet there is no agreement in the field on the best way of doing this, and thus we restrict ourselves to discussing the colour. Colour may be defined in terms of its chromaticity and its brightness or intensity. The intensity of our colour peaks are in line with the previously mentioned organic CLC Bragg filters[21] and higher than the recently developed inorganic Morpho colour technology.[10] We believe that the reflectance of a single CLC layer can be sufficient, not least based on how nature demonstrates that a single layer of cholesteric can give rise to very strong reflection colour in plants and animals, *e.g.*, in certain beetles that incorporate a CLC structure in their cuticles.[25] The chromaticities of our CLC coloured solar cells and the other technologies, based on the reflection spectra summarized in Fig. S6 (ESI†), are shown in Fig. 2(e) along with the s-RGB colour gamut. Our blue hued solar cells almost overlap with the vertices of the s-RGB gamut whilst our green and red hue are slightly further away, although still closer than Morpho colour.[10] This means that the ability to additively mix these fundamental colours by making small 'pixels' of single colour close to one another, following the same red-green-blue (RGB) colour mixing principle as used in digital display technology,[26] enables to make other colours, including non-spectral ones, resulting in a much wider colour palette, as we discuss in the next section.

Any colouring layer must be thermally stable since photovoltaic modules can operate at temperatures up to 70 °C, which is above the clearing transition of the unpolymerised CLC. To confirm that our samples sustain high temperatures, we subject the samples with blue, green and red retroreflection to temperatures up to 120 °C, finding only a slight blueshift of the peak from 100 °C and higher, see Fig. S7 (ESI†). To further validate the stability of the CLC layers we performed an aggressive damp heat test at 85 °C and 85% humidity, which is from the standard IEC 61215. We tested a red CLC layer by using an in-house humidity chamber (setup see Fig. S8, ESI†), with the edges exposed to the atmosphere, sandwiched between two pieces of glass for ten days under these conditions (the monitoring results are shown in Fig. S9, ESI†). Photography images of the film on day one before testing and on day ten are shown in Fig. 2(f), along with the reflection and transmission spectra. The film's optical properties remain unchanged within the error of measurement over the test period, as confirmed by the similarity of the two images. 240 hours testing is shorter than the standard 3000 hours usually needed for

Table 1 Comparison of the relative efficiencies of our work and previous works together with commercially available coloured PV modules. Note that the background has been coloured to match the colour of the cell or module derived from the respective reflection spectra (Fig. S6, ESI). For Heliartec these are colour codes RAL3028 (red), RAL6026 (green), RAL5015 (blue)

	Relative PCE (%)			
	Organic filters		Inorganic filters	Ceramic inks
	This work	Bae et al.[21]	Morpho[11]	HeliArtec[13]
Red	92.6	91.0	94.5	40.0
Green	93.6	93.0	94.3	32.5
Blue	96.3	95.0	94.4	42.5
Reference	100	100	100	100

guaranteeing a 25-year lifetime. However, for context, this is still sufficient time for an unencapsulated silicon module to degrade performance by 15% relative.[27] Here there was no colour change despite the edges of the CLC layer being exposed directly to the humid atmosphere. We are thus confident that the colour will be stable under all normal operating conditions. Although we have only demonstrated temperature stable constant red, green, and blue cells here, any spectral colour can be prepared in the same way simply by adjusting the amount of chiral dopant (see Methods).

Generating non-spectral colours with CLCs on solar cells

To go beyond spectral colours we subdivide the CLC coating into 'pixels' small enough not to be discriminated by the human eye at normal viewing distance, and we give each pixel one of the three fundamental colours red, green or blue. To do so, we now coat solar cells with reactive CLC mixtures that change colour across the visible spectrum depending upon their temperature (see Section SI 2.1, ESI† for the strategy behind the mixture development), and we photopolymerise them through photomasks at different temperatures, ensuring that only those pixels that have their target colour at the current temperature are irradiated by the UV light. The retroreflection colour of the unpolymerised mixture shifts continuously from blue to red on cooling (see Fig. S11, ESI†), from centre wavelength λ_0 = 461 nm at 66 °C to λ_0 = 685 nm at 10 °C. Adapting to this temperature dependence of λ_0, our pixelation procedure is shown in Fig. 3(a). After placing a drop of the mixture directly on the cleaned solar cell surface we heat to 66 °C and then cover it with the top glass. At this temperature, we UV-irradiate the sample through a photomask pre-designed with ~4 mm^2 transparent squares for all pixels that should be blue (see Methods). This polymerises the blue pixels into a strongly crosslinked solid polymer film while the remaining areas are still in a responsive CLC state. This allows us to cool the sample to 50 °C, a temperature where all unpolymerised CLC regions show green retroreflection. We now place a different photomask, again with ~4 mm^2 transparent squares for all pixels that should be green over the sample and UV-irradiate to make the green pixels permanent. After that, we decrease the

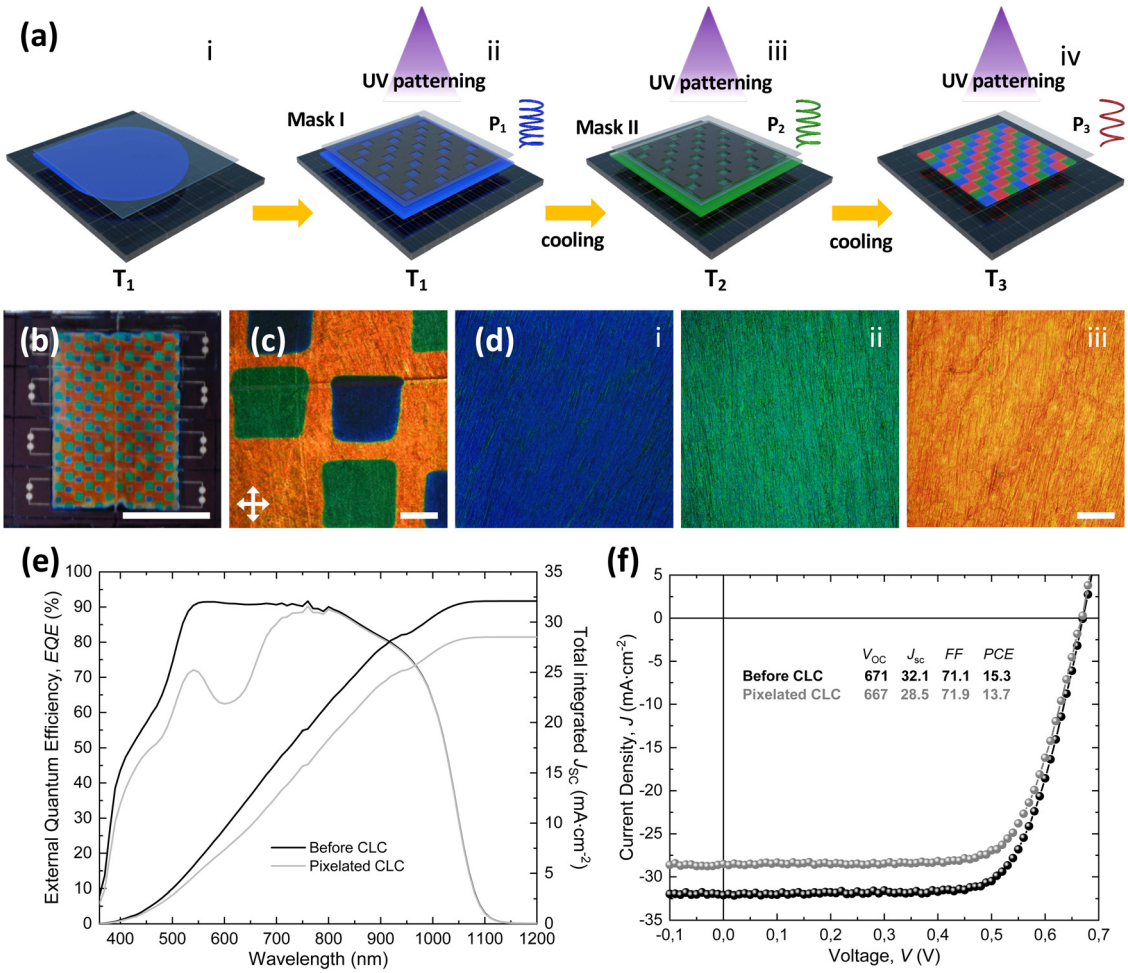

Fig. 3 (a) Schematic representation of the CLC film pixelation process. (b) Macroscopic photograph of orange-green-blue-pixellated solar cell. The contacts are left free for electrical measurements. (c) POM close-up images of the pattern (scale bar: 400 μm) and (d) each individual colour (scale bar: 100 μm). (e) The *EQE* spectra and integrated short circuit currents of the solar cell with and without pixellated CLC colours. (f) *JV*-curves of the solar cell before and after pixellated CLC coating, which are corrected according to the J_{SC} derived from *EQE* spectra.

temperature to 10 °C for the final curing, which does not require a mask since the only remaining unpolymerised regions are those that should become red pixels. Through these subsequent curing steps, we fix the retroreflection band centres within the three pixel types at 447 nm, 500 nm and 585 nm, respectively, as shown in Fig. S14 (ESI†). Our manually realised multi-step procedure is not perfect, leading to some deviation of the target colours, hence the red pixels end up rather orange, and their total area is slightly larger than the total areas of green and blue, respectively. If the sample is now subjected to heating or cooling, there is no longer any change in reflection colour since the CLC has been transformed into a highly crosslinked glassy film network. The result is that three permanent colours are alternatingly pixellated into small sizes of $\sim$1 mm^2 on the solar cell, as seen from the macro- and microscopic images in Fig. 3(b)–(d).

The *EQE* spectra of the solar cell before and after applying the pixellated CLC are demonstrated in Fig. 3(e). For the pixellated sample we show an average of five measurements conducted in regions of different colouring since the light beam size is only slightly larger than that of a pixel. As expected, before and after CLC coating, the *EQE* spectra are identical outside of the visible light region, the CLC-coated cell showing losses only due to the reflection of the CLC layer across all wavelengths with a distinct trough for the orange colour discernible. The loss across all visible wavelengths is expected since the reflection spectra (see Fig. S14, ESI†) are rather broad for each of the different colours. Based on the *EQE* from before and after pixelation, the J_{SC}^{EQE} is extracted to correct the respective *JV*-curves of these solar cells, as if they were fully covered with the pixellated CLC layer, as seen in Fig. 3(f). Furthermore, using a light beam with $\sim$400 μm diameter at the sample plane (μ*EQE* setup), the *EQE* spectra of individual pixels were recorded, confirming troughs for the orange, green and blue colours (see Fig. S15, ESI†).

As previously found for our uniformly coloured solar cells, the V_{OC} and FF of the pixellated solar cells remain almost the same within error when comparing before and after the addition of the CLC layer (see Fig. S13 and S12, ESI†). For the best cell the J_{SC}^{EQE} drops from 32.1 to 28.5 mA cm^{-2}, leading the pixellated sample to have a relative efficiency of 89% compared to before coating. Based on the sum-up of the reflection spectra for each individual pixel (see Fig. S14a, ESI†), it is obvious that the perceived colour from a distance moves towards the white part of the CIE diagram in Fig. S14a (ESI†). It is fair to compare relative efficiencies of our pixellated CLC solar cell and commercially available PV module with the nearest colour. Accordingly, we found the nearest colour of a window grey (RAL 7040) PV module from HeliArtec.[13] As shown in Table 2, the relative PCE of our pixellated solar cell is 50% relatively higher than that of commercial PV modules offering the similar colour.

Having demonstrated the minimal PCE loss also with pixellated CLCs capable of generating non-spectral colour on a 2 cm × 2 cm area of our solar cells, it is important to test at larger-scale if the pixelation allows the CLC coating to blend in with the urban environment. To this end, we create a 7.5 cm × 7.5 cm array of near identical polymerised CLC films with the same repeating RGB pattern as above, placed on black-painted microscope slides to emulate a PV module background, and photograph it in different environments and under varying lighting conditions as shown in Fig. 4. The sample is photographed at five different distances, approaching the camera stepwise from 6 m to 0.2 m to the sample. The backgrounds have been chosen based on two criteria: (1) their colours are non-spectral (and the two wooden surfaces are, additionally, textured), hence no conventional uniformly coloured CLC surface can be hidden on them by the principle of camouflage, and (2) their colours are close to the effective colour of our pixellated CLC array when seen over large distance under the lighting conditions of each photography series. Indeed, the sample is almost impossible to detect over distances greater than 2 m (i–iii), especially on the two wooden backgrounds where the effective colour is particularly suitable for providing camouflage. Against the silvery background of the metal plate the sample is detectable, but it is still well enough camouflaged that one would not notice it if not looking for it.

Table 2 Comparison of the best relative efficiency of the pixellated CLC and a commercially available grey coloured PV module (RAL 7040) from HeliArtec Corporation.[13] The specific colour of each has been indicated in the background, which is calculated for the pixellated device from the summed reflection spectrum

	Relative PCE (%)
pixellated CLC	89
HeliArtec	60

When the photography distance is less than 2 m (iv and v), the sample can be distinguished from the background in all cases. At these short distances, the sample is revealed also by the inability to place it flush with the background during these experiments, but this problem would disappear in a fully implemented BIPV context since each module becomes integrated in the façade. Note that we have not designed the pattern for any particular camouflage function, hence better results still can be expected when the pattern is purpose-designed, adapting it also for a much greater variety of backgrounds. Even with this very simple proof of concept, we have demonstrated that the pixellated polymerised CLC film can solve the first two problems of structural colour listed in the introduction, where the textured wooden backgrounds represent examples of patterned backgrounds. Moreover, pre-designing with various photomasks enables us to create arbitrary shapes, facilitating the production of intricate images. For example, the Christmas tree patterned solar cell shown in Fig. S16 (ESI†) is achieved using two photomasks and curing at different temperatures.

Concerning the third problem, which we do not address concretely in this paper, we study the sample appearance from different angles α with respect to the surface normal for each of the three situations of Fig. 4, see Fig. S17 (ESI†). We keep the distance approximately constant within one photography series, studying the sample on the wooden door at short distance (about 0.2 m) while the sample on the outdoor wall and door

Fig. 4 Photographs of a 7.5 cm by 7.5 cm array of RGB-pixellated polymerised CLC film placed on a wooden door and illuminated by indoor diffuse ambient light (top row), an outdoor wooden wall illuminated by indirect sunlight on a sunny day (middle row) and a silver-coloured metal panel on a door outside, also illuminated by indirect sunlight on a sunny day. For each situation, panels i to v are obtained with stepwise reduced photography distance, as indicated in the top row.

outside are studied at approximately 6 m distance. For reference, the normal-incidence appearance is included in the first column, whereas the other columns show the appearance at α = 20° to α = 60°. As α is increased, the apparent colour of the film blue shifts under all conditions, as expected. While the change in colour with viewing angle of this flat CLC film is clearly a drawback, one must remember that we have optimised the sample for normal viewing angle (retroreflection). Since the effective colour of each CLC pixel can be calculated using eqn (1), with appropriate averaging applied to account for diffuse illumination, and since it is so easy to change p by varying the mixture composition and/or the temperature of polymerisation, a tailor-designed BIPV coating based on our method would most likely not be designed based on retroreflection as in this first study, but rather on the most common viewing conditions that human occupants will experience. For instance, for an inclined roof, p would be extended in all pixels since no regular occupant will be observering it at normal incidence, and the same thing would apply for a BIPV module placed high above street level, where the apparent colour could be optimised for pedestrians who may observe the modules at an angle of $\theta \approx 60°$.

It is also possible to mold CLCs into spherical shape, polymerising each sphere into a solid and then distribute the resulting cholesteric spherical reflectors (CSRs) on a surface to create a reflective coating.[28,29] This has the great benefit that the viewing angle dependence is significantly reduced, yielding colours that are better defined regardless of illumination conditions and the orientation of the surface.[30] Moreover, since CSRs are effectively structural colour 'pixels' that can be distributed as desired across a surface, they are well suited to realise non-spectral colours by RGB color mixing.[31] Thus, polymerised CLCs have the potential to solve all three major drawbacks of current structurally coloured BIPV modules. However, the replacement of the flat CLC film with CSRs presents new challenges from a processing point of view that go well beyond the scope of this paper. While a method to pixelate a PV module surface using CSRs can certainly be developed, it would be more disruptive with respect to the current industrial PV module fabrication methods, whereas our current flat CLC film can readily be integrated with standard processes.

Integrated monitoring of solar cell operating temperature using unpolymerised CLCs

The thermochromic properties of CLCs can be exploited to make the colour of the solar cell change across the full visible spectrum as it heats and cools. This may find application as a way of monitoring the temperature of solar cells or modules, or even be used in a public health concept to warn people in real time of dangerously high air temperatures. The temperature-responsive CLC mixture used in this part of our study comprises the nematic LC mixture E7 and the chiral dopant S811

(chemical structures in Fig. S18, ESI†).[32,33] After thorough mixing at 80 °C (in the isotropic phase) to ensure homogeneity, a drop is placed onto the solar cell and then a protective cover glass is placed on top. As shown in Fig. 5(a), the solar cell with this CLC mixture exhibits blue retroreflection at 37 °C, corresponding to a peak at λ_0 = 470 nm (Fig. 5(b)). Upon gradually decreasing the temperature at a rate of −0.5 °C min^{-1} (Fig. S20 and Supplementary Video 1, ESI†), we induce a continuous redshift of the retroreflection colour until the sample appears red at 29.5 °C ($\lambda_0 \approx$ 680 nm). The reflection spectra are converted and placed on the CIE chromacity diagram in Fig. 5(c), clearly demonstrating colour in all parts of the visible spectrum. Visual observations and differential scanning calorimetry (DSC, see Fig. S19, ESI†) indicate that above 37 °C the CLC is in the isotropic phase, rendering it colourless, whilst below 29.5 °C the phase initially remains cholesteric but the retroreflection colour shifts into the infrared, thereby being invisible to the human eye.

To understand the effect of the colour modification by temperature change on the solar cell electrical performance, *EQE* measurements have been carried out at each temperature, as shown in Fig. 5(b). Again, the minimum in each individual *EQE* spectrum matches the maximum of the corresponding reflection spectrum. This is seen even for the near infrared response at 29 °C. As before, the width of the dip in *EQE* is larger at longer wavelengths, meaning that higher J_{SC} losses can be expected at longer wavelengths compared to shorter ones.

Fig. S21 and S22 (ESI†) visualise the comparison of the performance of the coloured solar cell as the temperature rises, and indeed once the solar cell is in the colouring temperature range, ≥29 °C, the J_{SC}^{EQE} steadily increases as the colour shifts from red to blue, whereas for uncoated CIGSe devices the current essentially stays constant.[34,35] The effect of increasing temperature leads to a well known decrease in the V_{OC} which is independent of the CLC layer[34,35] and the fill factor stays approximately constant as expected. Seemingly therefore, the CLC has no net adverse electrical effect on the solar cell and maintains 88–91.4% of its relative efficiency over the colouring temperature range as compared to room temperature.

To test the stability of the mixture and to check if the thermochromic behavior is reversible, the temperature sensitive CLC mixture is injected into a liquid crystal cell and placed in the in-house humidity chamber for five days. Afterward, the sample is tested for the reversibility of the colour change upon heating and cooling between 30 °C (red retroreflection) to 36.5 °C (blue retroreflection). As can be seen in Fig. 5(d), after

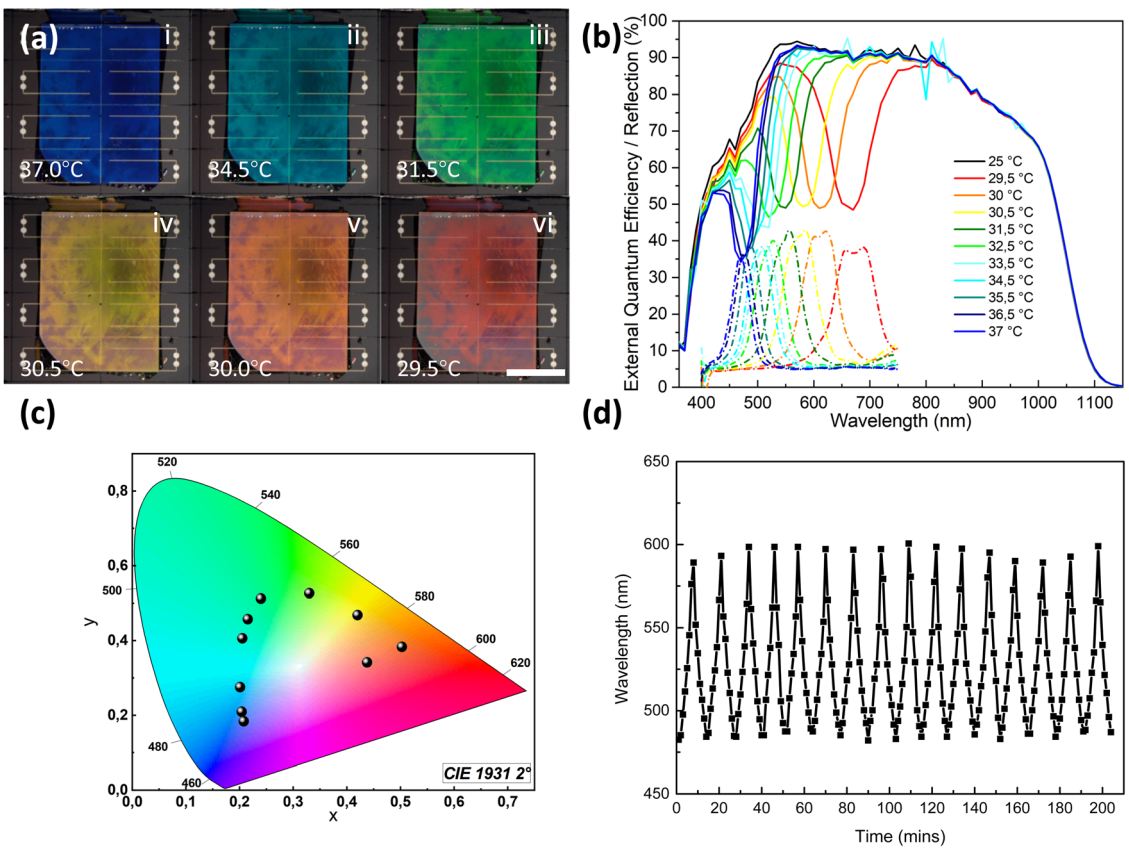

Fig. 5 (a) Macroscopic photographs of the solar cell with temperature-responsive CLC mixture. Scale bar: 1 cm. (b) Reflection spectra (dashed lines) and *EQE* measurements (continuous lines) of the solar cell with temperature-responsive CLC at various temperatures. (c) Colour coordinates (black dots) of this solar cell in the CIE 1931 2° chromaticity diagram, as obtained from the reflection spectra as the temperature decreased from 37 °C to 29.5 °C. (d) Reflection peak wavelength reversibility test result for temperature-responsive sample. The sample was first exposed to an environment of 85 °C and 85% humidity for five days, and then its reversibility is measured 16 times between 30 °C and 36.5 °C over two and a half hours.

16 cycles, the CLC peak reflection wavelength, and thus colour, exhibited constant reversibility. All things considered, the CLC mixture appears stable at elevated temperatures and the solar cells coated with temperature responsive CLCs perform as expected and have a dynamic decorative function.

Conclusion and outlook

We have shown that CIGSe solar cells can be directly coated with a constantly coloured fully polymerised CLC layer inside of the protective top glass ensuring its stability from the surrounding environment and without harming the solar cell's electrical properties. By extension, it is expected that the CLC would work equally well with market dominant silicon solar cells. The CLC colouring is agnostic to the PV technology as long as the naked solar cell has a black color. Due to the nature of CLCs the solar cells retain a high PCE since CLCs do not scatter or absorb light in the visible and near infrared parts of the solar spectrum. The colour of a CLC film was found to be unchanged after ten days of damp heat testing attesting to its stability. A further improvement in the colour of the devices can be expected when an alignment layer is utilized. The single colour films can be tuned to any colour of the spectrum by altering the concentration of chiral dopant. Alternatively, non-spectral colours may be formed by creating small pixels of spectral colours. While we here, for simplicity reasons, used photomasks to realise the pixellated structure, a faster and more versatile option is to use a digital light projector that can be programmed to irradiate each set of pixels specifically, without a mask. When coating these pixels on solar cells a similar high PCE was achieved, especially in comparison to the pigment alternatives, and when tested in a large-scale format, pixellated samples appeared to be indistinguishable from textured backgrounds with non-spectral colours at a distance of two metres or greater, aligning with the building materials commonly used by humans. This camouflaging could be tuned further by reducing the size of the pixels or by changing their number and distribution. By changing the mask, it is possible to create coloured images. Since CLCs are liquid, they may potentially be printed using more traditional methods in the future. Finally, CLC layers were made to actively change colour by using thermochromic sensitive mixtures over a 10 °C temperature range. By changing the chemistry, the exact temperature range where the colour transition occurs can be tuned giving them active functionality. With these innovations we offer a brighter, more colourful alternative view to the dark blue/black of traditional solar modules, thereby increasing the likelihood of public acceptance.

Methods

Device fabrication

$Cu(In,Ga)Se_2$ (CIGSe) absorber layers were co-evaporated using a 3-stage deposition process on 400 nm thick molybdenum coated pre-cleaned soda lime glass with the size of 25 × 25 × 2 mm^3. The final thickness of absorbers is approximately 2.5 μm. The samples show Cu-poor composition with a final molar fraction ratio of Cu/(Ga + In) of 0.9. More details regarding the 3-stage process can be found in Choubrac *et al.*.[36] Following the etching of the CIGSe absorber layers with an aqueous 5% $KCN_{(aq)}$ solution for 30 seconds, a CdS buffer layer was deposited by chemical bath deposition. Window layers consisting of an intrinsic ZnO and a doped ZnO:Al (transparent conductive oxide) are sputtered. Ni–Al contact grids were e-beam evaporated in order to facilitate current collection.

Current density–voltage (*JV*) measurement

JV measurements have been conducted under standard test conditions (STC) of AM1.5G, 0.1 W cm^{-2}, 25 °C in a 4-point probe configuration using an AAA class sun simulator. The sun simulator is calibrated by a silicon reference solar cell with a tolerance of ± 2%. In case of temperature responsive CLCs applied on solar cells, the solar cells could not be measured anymore under STC due to the changes in temperature. Prior to each measurement, a contact resistance is ensured to be below 2 Ω cm^2. It is worth noting that *JV* measurements provide the total area efficiency of the solar cells with some uncertainty. The uncertainty arises from the incomplete coverage of CLC colouring layers on top of solar cells with slightly different areas, and the shadowing effect of the front contacts. To obtain a more accurate representation of the solar cell's PCE, it is essential to correct the J_{SC}^{JV} measured by the *JV*-measurement by using J_{SC}^{EQE} derived from *EQE* measurements, enabling to calculate the active area efficiency. This enables us to calculate the current as if the entire surface of the solar cells is covered with the CLC colouring layer, ensuring a more precise evaluation of the CLC colouring potential. Regarding the correction of J_{SC}^{JV} with J_{SC}^{EQE}, the correction factor J_{SC}^{EQE}/J_{SC}^{JV} is multiplied by all *J*-values for respective voltage values, thereby adjusting the entire *JV*-curve. Subsequently, the performance parameters are recalculated using the corrected data. Please refer to Section SI 1.1 and Fig. S2f (ESI†) for further information.

External quantum efficiency (*EQE*) measurement

EQE measurements using an in-house built setup were performed in a dark environment. Based on the *EQE*-spectra of a solar cell, the total integrated short circuit current density can be extracted according to the AM1.5G solar irradiance. It is worth noting that the standard size of the *EQE*-measurement spot is around 1 mm in diameter. For the measurement of the pixellated solar cells the *EQE* was measured five times on the same solar cell with 0.5 mm intervals along the *x* coordinate. To investigate the *EQE* of the individual pixels, the *EQE*-measurement spot was focused down to ~400 μm in diameter, such that it only probes the current generated from a single pixel. Furthermore, the solar cells employed for the permanent CLC-generated single colours have a band gap of 1.17 eV, as determined from the inflection point of *EQE* curve ($dEQE/d\lambda$). The solar cells employed in the remaining sections have a band gap of 1.19 eV. The discrepancy in E_g between solar cells, and the slightly different interference fringes from different batches is responsible for the observed differences in J_{SC} among these reference solar cells.

CIE 1931 2° chromaticity diagram

A CIE 1931 2° chromaticity diagram with D65 illuminant was created using Origin(Pro) 2020 data analysis and graphing software based on the reflection spectra of the coloured samples or literature references.

Fabrication of colour films

The CLC for a permanent colour film was a mixture of (chemical structures shown in Fig. S1, ESI†) 4-hex-5-enyloxy-biphenyl-4-carbonitrile (6OCB-1-ene, Synthon Chemicals, purity: 98%), 1,4-bis-[4-(3-acryloyloxypropyloxy)benzoyloxy]-2-methylbenzene (RM257, Wilshire Technologies, purity: 95%), R5011 (chiral dopant, HCCH, China, purity: 99.5%) and 2,2 dimethoxy-2-phenylacetophenone (photoinitiator Irg651, Sigma Aldrich, purity: 99%) at mass ratios shown in the top row of Table S1 (ESI†). In order to tune the colour of the film, varying amounts of chiral dopant were added.

The mixture applied to fabricate the non-spectral coloured film is prepared from a polymerisable temperature-dependent liquid crystal mixture (chemical structures shown in Fig. S10, ESI†). Inspired by de Haan *et al.*,[37] the Schröder-van Laar equation was used for formulating a eutectic mixture, adjusting the proportion of monomers with carboxylic acid endings to expand the temperature range of LC phase and reflection interval.[38] The CLC mixture is composed of 1,4-bis[4-(6-acryloyloxyhexyloxy)-benzoyloxy]-2-methylbenzene (RM82, Wilshire Technologies, purity: 95%), (3*R*,3a*S*,6a*S*)-hexahydrofuro[3,2-*b*]furan-3,6-diyl bis(4-(4-((4-(acryloyloxy)butoxy)carbonyloxy)benzoyloxy)benzoate) (LC756, Synthon Chemicals, purity: 90%), 4-(3-acryloyloxy-*n*-prop-1-yloxy)-benzoic acid (BA-3, Synthon Chemicals, purity: 96%), 4-(5-acryloxy-pentyl-1-oxy)benzoic acid (BA-5, Synthon Chemicals, purity: 96%), 4-(6-acryloyloxy-*n*-hex-1-yloxy)benzoic acid (BA-6, Synthon Chemicals, purity: 96%), 4-methoxybenzoic acid 4-(6-acryloyloxy-hexyloxy)phenyl ester (RM105, Synthon Chemicals, purity: 98.5%),and 2,2 dimethoxy-2-phenylacetophenone (photoinitiator Irg651, Sigma Aldrich, purity: 99%), the mass ratios shown in Table S2 (ESI†). The temperature-responsive CLC film was a mixture of (chemical structures shown in Fig. S18, ESI†) commercial nematic LC E7 (HCCH, china, purity: 99.5%) and S811 (chiral dopant, HCCH, china, purity: 99.5%) at mass ratios shown in Table S3 (ESI†).

The mixtures were magnetically stirred at 80 °C for around 5 h to ensure that all the components were homogeneously mixed. To achieve the three permanent spectral colours, each respective mixture was first cooled to 40 °C and kept at this temperature for 1 h before use. Three protective top glass plates were placed on two adjacent solar cells, using glue along two parallel sides of the glass. By including spacer balls in the glue we fixed the solar cell-to-protective glass spacing to 15 μm. We then place a drop of each reactive CLC mixture at an edge without glue, such that it can fill the entire area by capillary force, and then the sample was placed in a UV-curing chamber (Opsytec Dr Gröbel Irradiation Chamber BSL-01) for about 1 min for UV polymerisation, with the wavelengths 330–450 nm and irradiation intensity of 200 mW cm^{-2} at the sample plane. The experimental procedures are shown in Fig. S2 (ESI†). The procedure for generating non-spectral colours with CLCs on solar cells is shown in Fig. 3(a). The mixture was dripped onto the solar cells at 66 °C, then covered with glass and left to anneal for 5 min. A pre-designed photomask was placed on the glass surface and a handheld UV-LED system (30W IP66 Onforuled, China) was used for photopolymerisation. The photomasks were obtained by printing two pre-designed black patterns on a PET substrate with a laser printer. The appearance of the square photomask (18 by ~18 mm^2) was like a grid-like checkerboard and comprised of ~4 mm^2 small squares, with 27 transparent and 54 black squares. Every two black squares were separated by a transparent one. The difference between the two photomasks was that the transparent square was sequentially shifted to ensure that the sample was not repeatedly exposed in the same place. After 10 s UV exposure with an intensity of 30 W cm^{-2}, the sample was cooled down to 50 °C at 5 °C min^{-1}. After stabilisation for 5 min, the first photomask was replaced by the second photomask, followed by 10 s of photopolymerisation. Finally, the photomask was removed and the sample was cooled down to 10 °C for another 10 s UV exposure.

The morphological appearance and reflection features of each sample were observed using an Olympus BX51 reflection polarising optical microscope equipped with a digital camera (Olympus DP73). The reflection spectra of each sample were measured by using unpolarised white illumination and an Avantes AvaSpec-2048 spectrophotometer, connected directly to the microscope. The phase sequences of the temperature-responsive LC mixture were investigated by a differential scanning calorimeter (DSC823 Mettler Toledo, USA) with a scanning rate of 5 °C min^{-1} between 0 and 50 °C in a nitrogen atmosphere. Macroscopic images and videos were acquired with a Canon EOS 100D camera. The environmental stability of a permanent constant colour layer and the temperature-sensitive CLC film were tested according to 85 °C and 85% humidity in line with a test from the IEC 61215 standard. See Section SI 1.7 (ESI†) for details.

Author contributions statement

PD and JL developed the concept for the study and supervised the work. YZ, HAY, JL and PD wrote the manuscript. RK and LM conducted critical pilot experiments for the study. RK initially prepared the CLC mixtures. LM made initial solar cell measurements. HA integrated the CLC mixtures for single colour solar cells and developed the initial pixellation work. YZ further developed the CLC mixtures and integrated them into all the types of coloured solar cells, and did most of the optical characterisation and metrology. HAY performed and analysed most of the electrical and opto-electronic measurements. RP performed micro-*EQE* measurements on the individual coloured pixels. SG synthesised the CIGSe absorber layers. All authors revised the manuscript.

Data availability

All raw data supporting the findings of this study are openly available at zenodo.org *via* the DOI: **10.5281/zenodo.14258128**.

Conflicts of interest

PD, JL, HAY, YZ, HA have filed a patent application, LU507448, based on the pixellated solar cell results.

Acknowledgements

We thank Dr Yong Geng and Clara Schreck for fruitful discussions. We acknowledge Michele Melchiorre for completing the fabrication of solar cells. Financial support from University of Luxembourg is gratefully acknowledged. SG and RP gratefully acknowledge the funding from the Luxembourg National Research Fund (FNR) with the grant reference C20/MS/14735144/TAILS and PRIDE17/12246511/PACE, respectively.

References

1 IPCC. Climate Change 2022: Mitigation of Climate Change. Contribution of Working Group III to the Sixth Assessment Report of the Intergovernmental Panel on Climate Change (Cambridge University Press, Cambridge, UK and New York, NY, USA, 2022).
2 C. Breyer, *et al.*, Reflecting the energy transition from a European perspective and in the global context—Relevance of solar photovoltaics benchmarking two ambitious scenarios, *Prog. Photovoltaics: Res. Appl.*, 2022, **31**(12), 1369–1395.
3 M. Z. Jacobson, *et al.*, Low-cost solutions to global warming, air pollution, and energy insecurity for 145 countries, *Energy Environ. Sci.*, 2022, **15**, 3343–3359.
4 Eurostat. How much of your region is covered by man-made surfaces? (2018) **https://ec.europa.eu/eurostat/web/products-eurostat-news/-/WDN-20180523-1%7D** (accessed May 2024).
5 H. S. Boudet, Public perceptions of and responses to new energy technologies, *Nat. Energy*, 2019, **4**, 446–455.
6 A. Feige, H. Wallbaum and S. Krank, Harnessing stakeholder motivation: towards a swiss sustainable building sector, *Build. Res. Inf.*, 2011, **39**, 504–517.
7 E. Commission, *Energy efficiency in buildings*, 2020, **https://commission.europa.eu/news/focus-energy-efficiency-buildings-2020-02-17_en**, (accessed May 2024).
8 Energy. Office of energy efficiency & renewable energy (2024), **https://www.energy.gov/eere/buildings/about-building-technologies-office** (accessed May 2024).
9 C. Ballif, L.-E. Perret-Aebi, S. Lufkin and E. Rey, Integrated thinking for photovoltaics in buildings, *Nat. Energy*, 2018, **3**, 438–442.
10 J. Eisenlohr, *et al.*, Highly efficient coloured BIPV modules with anti-glare properties, *13th Conference on Advanced Building Skins 2018*, 2018.
11 B. Bläsi, T. Kroyer, T. E. Kuhn and O. Höhn, The morpho-color concept for colored photovoltaic modules, *IEEE J. Photovolt.*, 2021, **11**, 1305–1311.
12 Kameleon solar technology (2024), **https://kameleonsolar.com** (accessed May 2024).
13 Heliartec solutions corporation (2024), **https://heliartec.com**, (accessed May 2024).
14 P.-G. De Gennes and J. Prost, *The physics of liquid crystals*, Oxford university press, 1993.
15 H. Kitzerow and C. Bahr, *Chirality in Liquid Crystals (Partially Ordered Systems)*, Springer, 2000.
16 J. Alamán, R. Alicante, J. I. Peña and C. Sánchez-Somolinos, Inkjet printing of functional materials for optical and photonic applications, *Materials*, 2016, **9**, E910.
17 C. Jones, F. J. Wortmann, H. F. Gleeson and S. G. Yeates, Textile materials inspired by structural colour in nature, *RSC Adv.*, 2020, **10**, 24362–24367.
18 C. Williams, R. Parker, A. Kyriacou, M. Murace and S. Vignolini, Inkjet printed photonic cellulose nanocrystal patterns, *Adv. Mater.*, 2023, **36**(1), 2307563.
19 D. Broer, G. P. Crawford and S. Zumer, *Cross-linked Liquid Crystalline Systems: From Rigid Polymer Networks to Elastomers*, CRC press, 2011.
20 X. Zhang, *et al.*, Liquid crystal-templated chiral nanomaterials: from chiral plasmonics to circularly polarized luminescence, *Light: Sci. Appl.*, 2022, **11**, 223.
21 S. Bae, Y. W. Noh, D.-S. Park, M. H. Song and S.-W. Choi, Development of colored perovskite solar cells using cholesteric helicoidal superstructures, *Nano Energy*, 2022, **93**, 106801.
22 G. Peharz and A. Ulm, Quantifying the influence of colors on the performance of c-si photovoltaic devices, *Renewable Energy*, 2018, **129**, 299–308.
23 J. Halme and P. Mäkinen, Theoretical efficiency limits of ideal coloured opaque photovoltaics, *Energy Environ. Sci.*, 2019, **12**, 1274–1285.
24 A. Røyset, T. Kolås and B. P. Jelle, Coloured building integrated photovoltaics: Influence on energy efficiency, *Energy Build.*, 2020, **208**, 109623.
25 R. R. da Rosa, S. N. Fernandes, M. Mitov and M. H. Godinho, Cellulose and chitin twisted structures: From nature to applications, *Adv. Funct. Mater.*, 2023, **34**(35), DOI: **10.1002/adfm.202304286**.
26 *Color management in the real world: sRGB, ICM2, ICC, ColorSync, and other attempts to make color management transparent*, ed. B. E. Rogowitz, and T. N. Pappas, SPIE, 1998.
27 W. Liu, *et al.*, Damp-heat-stable, high-efficiency, industrial-size silicon heterojunction solar cells, *Joule*, 2020, **4**, 913–927.
28 Y. Geng, R. Kizhakidathazhath and J. P. F. Lagerwall, Encoding hidden information onto surfaces using polymerized cholesteric spherical reflectors, *Adv. Funct. Mater.*, 2021, **31**, 2100399.
29 A. Belmonte, T. Bus, D. Broer and A. Schenning, Patterned full-color reflective coatings based on photonic cholesteric liquid-crystalline particles, *ACS Appl. Mater. Interfaces*, 2019, **11**, 14376–14382.
30 H. Agha, *et al.*, Unclonable human-invisible machine vision markers leveraging the omnidirectional chiral Bragg diffraction of cholesteric spherical reflectors, *Light: Sci. Appl.*, 2022, **11**, 309.
31 H. Agha, Y.-S. Zhang, Y. Geng and J. P. F. Lagerwall, Pixelating structural color with cholesteric spherical reflectors, *Adv. Photonics Res.*, 2023, **4**, 2200363.
32 S.-A. Jiang, *et al.*, Toward full-color tunable chiroptical electrothermochromic devices based on a supramolecular chiral photonic material, *Adv. Opt. Mater.*, 2021, **9**, 2001796.

33 F. Zhang and D.-K. Yang, Temperature dependence of pitch and twist elastic constant in a cholesteric to smectic a phase transition, *Liq. Cryst.*, 2002, **29**, 1497–1501.
34 M. Theelen, *et al.*, Determination of the temperature dependency of the electrical parameters of CIGS solar cells, *J. Renewable Sustainable Energy*, 2017, **9**, 13.
35 H. Ahmed, *et al.*, Temperature coefficient characterization of CIGSSe solar cells with layer modifications, *Sol. Energy Mater. Sol. Cells*, 2021, **225**, 111059.
36 L. Choubrac, T. Bertram, H. Elanzeery and S. Siebentritt, Cu(In,Ga)Se_2 solar cells with improved current based on surface treated stoichiometric absorbers, *Phys. Status Solidi A*, 2017, **214**, 1600482.
37 L. T. de Haan, J. M. Verjans, D. J. Broer, C. W. Bastiaansen and A. P. Schenning, Humidity-responsive liquid crystalline polymer actuators with an asymmetry in the molecular trigger that bend, fold, and curl, *J. Am. Chem. Soc.*, 2014, **136**, 10585–10588.
38 J. Bao, *et al.*, Freestanding helical nanostructured chiro-photonic crystal film and anticounterfeiting label enabled by a cholesterol-grafted light-driven molecular motor, *Small Methods*, 2022, **6**, 2200269.

